Rubber Content Effect on Scratch Behavior in Acrylonitrile-Styrene-Acrylate Copolymers

Yi-Ling Liang,[1] Hung-Jue Sue,[1] Rolf Minkwitz[2]

[1]*Polymer Technology Center, Department of Mechanical Engineering, Texas A&M University, College Station, Texas 77843-3123*
[2]*BASF SE, Ludwigshafen, Germany*

Received 10 August 2011; accepted 11 January 2012
DOI 10.1002/app.36801
Published online in Wiley Online Library (wileyonlinelibrary.com).

ABSTRACT: The scratch behavior of butyl-acrylate rubber-modified styrene-acrylonitrile thermoplastics is investigated following the ASTM D7027 linearly increasing normal load test methodology. The critical normal loads at the onset of the major transitions along the scratch path, such as groove formation, scratch visibility, microcrack formation, and plowing, are reported and quantitatively analyzed. It is found that the scratch resistance generally deteriorates with increasing butyl-acrylate rubber content, and is strongly related to the tensile and compressive yield stresses of the blends. Microscopy investigation indicates that a rubber content of up to 30 wt % in a styrene-acrylonitrile copolymer (SAN) does not alter the scratch-induced damage mechanisms, but only reduces the critical onset loads for the observed damage transitions. The present finding suggests that addition of rubber causes reductions in modulus, tensile, and compressive yield stresses, thus leading to deterioration in scratch resistance. It appears that the improvement in ductility for SAN after the rubber toughening does not benefit scratch resistance. Implication of rubber toughening on scratch behavior of polymers is discussed. © 2012 Wiley Periodicals, Inc. J Appl Polym Sci 000: 000–000, 2012

Key words: scratch behavior; acrylonitrile-styrene-acrylate; rubber content; structure–property relationship

INTRODUCTION

The aesthetic appearance of thermoplastics has become an important property of concern in recent years. One approach to rank aesthetic property of polymers is to compare their resistance against scratch-induced material deformations. Although numerous polymer scratch studies have been carried out,[1–17] fundamental knowledge on polymer scratch behavior is still lacking. In particular, it is still uncertain whether rubber particles employed in most thermoplastic applications as impact-modifiers can help improve scratch resistance of polymers. Even though rubber particles are typically known for their effectiveness in enhancing ductility and toughness of the polymer matrix, they can reduce matrix modulus and strength.[18,19] Therefore, it would be of interest to fundamentally study the impact of rubber particles on the scratch behavior of polymers.

Scratch deformation, which is defined in this context as the deformation caused by a single path scratching process, can be considered as a form of abrasion in tribology.[1] Although a variety of experimental techniques have been proposed for polymer scratch testing since 1950,[2–6] only recently was a standardized test methodology established and designated as the ASTM D7027-05 method.[7] Employing this ASTM standard, several quantitative scratch performance evaluation and structure–property relationship investigations have been carried out.[7–14] By applying a progressive normal load, this scratch test generates scratch deformations with distinctive damage transitions throughout the scratch path. These transitions may include groove formation, scratch visibility transition, fish-scale development, microcracking, and plowing.[13] Identification and analysis of these damage transitions is important for fundamental understanding of scratch behavior of polymers.

Several attempts have been made to categorize the observed damage features into scratch-deformation maps. Briscoe et al.[15,16] pointed out that the formation of scratch damage features in the same polymers depends on the normal load, testing speed, testing temperature, and the cone angle of the scratch tip. Maeda et al.[17] emphasized the relationship between the friction force and scratch damages by manipulating the cone angle of the scratch tips and the viscoelastic properties of formulated rubber compounds. Recently, Jiang et al.[13] investigated four

Correspondence to: H.-J. Sue (hjsue@tamu.edu).
Contract grant sponsors: BASF SE.

kinds of distinctively different commercial polymers and detailed the relationship between material characteristics and scratch deformation features. These scratch maps are useful for illustrating the importance of various material parameters and testing conditions on scratch damage mechanisms.

Jiang et al.[13] also provided an in-depth mechanistic description on how the scratch damage evolves. By using a three-dimensional finite element analysis, they found that the material beneath the scratch tip experiences a compressive stress state while the material element behind the scratch tip experiences tensile stress in an early stage of scratch, which either leads to fish-scale formation in the case of ductile polymers or crazing/microcracking in the case of brittle polymers. They also noticed an additional maximal tensile stress component develops in front of the scratch tip as the normal load increases, which eventually leads to plowing or cutting as the exerted stress magnitude exceeds the strength of the material. The aforementioned numerical findings are beneficial in the interpretation of why and how certain deformation mechanisms are observed.

Polymeric materials usually consist of more than one chemical component and can be multi-phase in nature. As a result, choices of processing equipment and conditions can significantly affect their final phase morphology and skin-core characteristics. In a recent study on a soft thermoplastic olefin (TPO) that consists of 70 wt % ethylene-propylene rubber (EPR) and 30 wt % polypropylene (PP), Browning et al.[11] found that the crystallinity of the ethylene segment and the internal morphology of the EPR phase significantly affect the scratch behavior of the soft TPO. In another study, Moghbelli et al.[12] manipulated the skin-core morphology of PP thin sheets through post-processing thermal treatments. Their results suggest that the degree of surface crystallinity can significantly influence the scratch behavior. Moghbelli et al.[14] further showed that neat epoxy resin exhibits a higher scratch resistance than nanocomposites of the same epoxy filled with either ZrP nanoplatelets or core-shell rubber (CSR) nanoparticles. This implies that the improvements in tensile strength and modulus alone (i.e., epoxy/nanoplatelet scenario) or fracture toughness and ductility alone (i.e., epoxy/CSR scenario) may not necessarily lead to the enhancement of scratch performance.

The main objective of this work is to investigate the rubber content effect on the scratch behavior. For this purpose, an amorphous thermoplastic polymer is preferred, which avoids complexity of crystallinity and severe skin-core morphology effects. An amorphous styrene acrylonitrile (SAN) matrix with known scratch properties[1] and butyl-acrylate as rubber phase were chosen. This polymer class, abbreviated as ASA in the technical literature, is considered to be a weather-resistant counterpart of acrylonitrile-butadiene-styrene (ABS) terpolymer. ASA is usually employed in exterior applications, such as automotive radiator grills[20] and its annual production is estimated to be roughly 250 kT in 2010.[20,21]

EXPERIMENTAL

Materials

The ASA polymers were provided by BASF SE (Ludwigshafen, Germany). The ASA polymers consist of a random copolymer matrix of SAN and grafted poly(*n*-butyl acrylate) (PBA) rubber particles with an average nominal diameter of 475 nm, which is also known as poly(BA)-*graft*-poly(SAN). The PBA rubber content in ASAs was varied from 0 to 30 wt % (Table I). In the SAN phase, the ratio of acrylonitrile was controlled at 35 wt % and the M_w of the SAN was 104 kg/mol as obtained by light scattering measurements. Color pigments of 0.325% of anthrachinone and 0.15% of pyrazolone yellow were blended into the resins to provide adequate color background for the scratch visibility investigation.

The test specimens were fabricated by injection molding with a fan gate design to spread and slow the melt as it enters the mold cavity. The plaques were rectangular with dimensions of 150 mm × 150 mm × 6 mm. Prior to scratch testing, the specimens were dried in a vacuum oven at 86°C for 24 h to remove any pre-existing moisture to minimize possible moisture effect on scratch behavior.[1] Afterwards, the specimens were annealed between two smooth glass plates at 108°C for 2 h under vacuum and allowed to slowly cool in a vacuum oven to minimize any residual stresses caused by the injection molding process. The scratch tests were completed within an hour of annealing to minimize moisture adsorption from atmosphere.

Transmission electron microscope

The rubber particle dispersion investigation was carried out at BASF SE (Ludwigshafen, Germany) via transmission electron microscope (TEM). The samples were cryo-microtomed with a Leica EM UM 6 microtome at −120°C, contrasted with RuO_4 and imaged using a Zeiss LIBRA 120 TEM at 120 kV.

Differential scanning calorimetry

The glass transition temperature was measured with a Mettler Toledo DSC821 using a temperature range of 30–150°C. A heating rate of 10 °C/min was chosen and an inert nitrogen gas flow was controlled at a rate of 80 mL/min.

TABLE I
The Rubber Content and Surface Characteristics of the Model ASA Systems

Denotation	Rubber content (wt %)	60° specular gloss (%, $n = 3$)		R_q (μm, $n = 3$)	
		As received	After annealing	As received	After annealing
ASA1	6	95.1 ± 0.6	93.0 ± 1.3	0.95 ± 0.11	0.91 ± 0.10
ASA2	12	91.7 ± 0.5	88.6 ± 2.1	0.96 ± 0.12	1.03 ± 0.11
ASA3	18	86.1 ± 0.9	84.6 ± 1.6	1.04 ± 0.54	1.08 ± 0.11
ASA4	24	77.2 ± 1.4	77.4 ± 0.6	1.22 ± 0.02	1.33 ± 0.06
ASA5	30	71.3 ± 1.1	71.2 ± 0.5	1.56 ± 0.05	1.46 ± 0.08

R_q denotes the root-mean-square surface roughness, which is based on the measurement performed using VLSCM in a sampling area of 1.3 × 1.0 mm^2.

Surface finish

A 60° specular gloss and the root-mean-square surface roughness (R_q) were obtained using BYK Gardner® Micro-TRI Glossmeter and Keyence® VK9700 violet laser scanning confocal microscope (VLSCM), respectively. The reported values were calculated based on an average of three measurements.

Mechanical property characterization

The tensile test was conducted by BASF SE (Ludwigshafen, Germany). The dimensions of the dog-bone shape specimens were based on ASTM D638 type I geometry.[22] The nominal overall length, thickness, and width of the narrow section were 170, 4, and 10 mm, respectively. The test was performed at a constant speed of 50 mm/min under ambient temperature.

The uniaxial compression tests were performed following the ASTM standard D695[23] using a screw-driven load frame (MTS® Insight) and an MTS® extensometer with a gauge length of 25.4 mm. The compression specimens were precisely cut by an Isomet® Precision Saw 1000 into prisms with sharp clean edges. The nominal dimensions of the prisms were 12.7 mm × 6 mm × 6 mm, and the actual dimensions were measured by a digital caliper. The surfaces of the specimens were carefully polished using 4000 grit silicon carbide polishing paper, and adequate lubricant (Dupont® Teflon™ Silicone Lubricant spray) was also applied on the contact surfaces between the mechanical apparatus and the testing samples to reduce surface friction. The compression tests were performed at a crosshead speed of 2.5 mm/min under ambient temperature.

Scratch tests

Scratch tests were performed under ambient temperature following the ASTM D7027-05 scratch testing method.[24] The scratch tip was made of stainless steel and had a 1 mm diameter spherical geometry. The scratch direction was chosen in the same direction as the melt flow during molding for all the tests. A progressive load of 1–80 N at constant scratch speeds of 1, 10, and 100 mm/s was used to evaluate the scratch performance over a length of 100 mm. Note that a 10-mm lead distance at 1 N constant load was used at 100 mm/s scratch speed to reduce the inertial effect as the linearly increasing normal load was applied to the specimen.

Post-scratch analysis

In order to provide sufficient time for viscoelastic recovery after the scratch test, the sample damage features were characterized after 24 h upon completion of the scratch tests. The optical microscopy images and the topographical information were obtained by using the aforementioned VLSCM and its accompanied image analysis software (VK Analyzer, 2.1.0, Keyence). For the scratch visibility analysis, a commercially available software ASV© (Automatic Scratch Visualization, http://www.surfacemachines.com) was applied. The scanned scratch images for analysis were obtained by using a PC scanner (Epson® Perfection Photo 4870) at 300 dpi resolution under "no color correction" mode. For all scanned images, the scratch direction was aligned perpendicular to the scanner light source movement. Additional characterization details can be found elsewhere.[1]

RESULTS AND DISCUSSION

Rubber particle dispersion

ASA is a polymer blend similar to ABS, but exhibiting good weatherability due to the lack of C=C double bonds in the rubber.[20] The TEM images of the blends display a typical dispersion and size characteristics of the rubber in SAN matrix (Fig. 1).

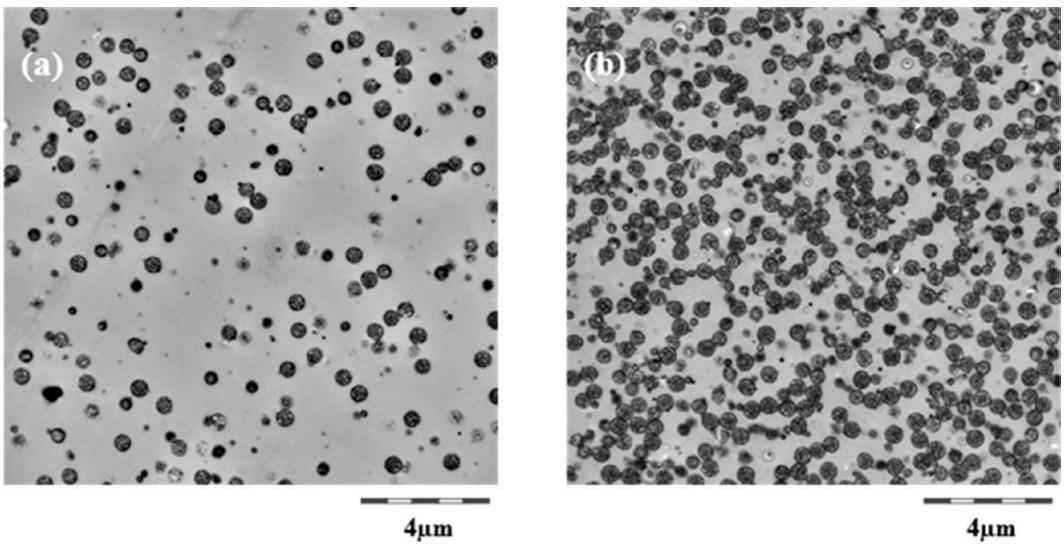

Figure 1 TEM images of (a) ASA1 and (b) ASA5. The rubber phase has a dark appearance in the images.

Annealing and surface finish

The T_g of ASAs measured by differential scanning calorimetry (DSC) in the present study is similar to the reported values at 110°C.[25] Investigation of the surface characteristics on both sides of the post-annealed ASA plaques indicates that the top side of each plaque, which was not directly exposed to the heat source during the annealing process, shows similar surface finish characteristics to the as-received samples (Table I). Hence, the top surface of each plaque was used for further scratch tests and evaluation.

Bulk mechanical properties

The stress–strain curves obtained from uniaxial tensile and compressive tests of all the ASA systems as well as neat SAN are shown in Figures 2 and 3. As expected, increasing the PBA rubber content results in an increase in elongation at break, while reducing the matrix tensile and compressive yield stress as well as Young's modulus.

Scratch damage analysis

Figure 4 illustrates a schematic of typical scratch damage features observed in an ASA system. Under progressive normal loading conditions, the scratch damage in ASAs gradually develops from subtle to conspicuous. The damage features observed by using VLSCM can be categorized into three major deformation transitions: (1) the onset of groove formation, (2) the onset of periodic cracking, and (3) the onset of plowing. It should be noted that the onset of groove formation represents a subtle plastic

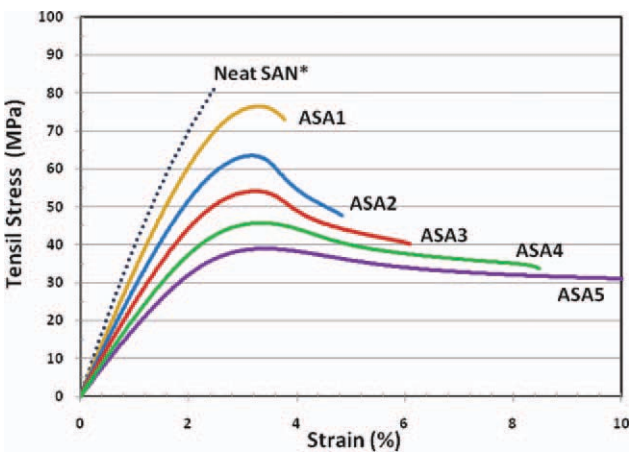

Figure 2 Stress–strain curves of ASAs obtained from tensile tests and compared to the literature of neat SAN.[1] [Color figure can be viewed in the online issue, which is available at wileyonlinelibrary.com.]

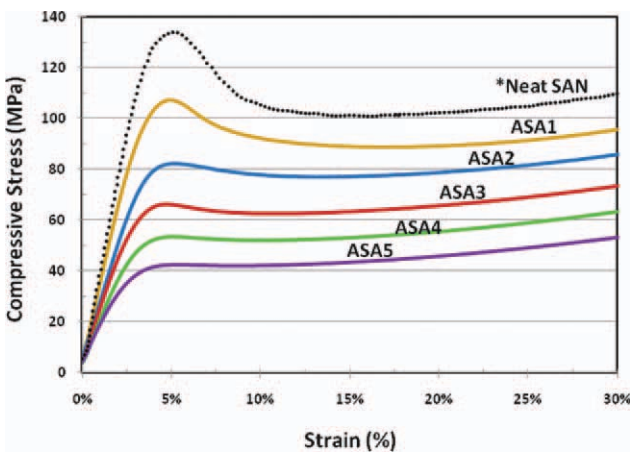

Figure 3 Compressive stress–strain curves of ASAs and compared to the literature of neat SAN.[1] [Color figure can be viewed in the online issue, which is available at wileyonlinelibrary.com.]

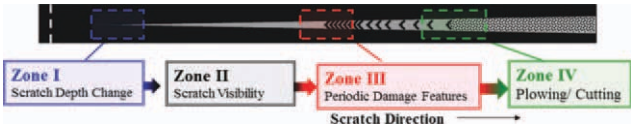

Figure 4 A schematic drawing shows typical deformation transitions seen in ASA under progressive normal load scratch.[1] [Color figure can be viewed in the online issue, which is available at wileyonlinelibrary.com.]

deformation feature developed during an early stage of the scratch process, while the onsets of cracking and plowing are indicators of material failure on the surface beyond which material removal begins to take place. Also, note that the onset of scratch visibility in these ASA systems is always found to be between the onset of groove formation region and the periodic cracking region, which will be discussed later.

Onset of groove formation

Figure 5 includes the typical height contour plots along the scratch path. It can be seen that the scratch groove is much deeper for ASA5 than ASA1 at 1 mm/s scratch testing speed. The onset of groove formation was further analyzed based on the comparison between the virgin and post-mortem scratch profiles. Figure 6 represents a typical quantitative analysis of scratch depth profiles as a function of the applied normal load. As shown in Figure 6, the first sign of measured height deviation between the intact surface and the scratch depth can be accurately determined, and the corresponding normal load is reported as the critical load for onset of groove formation.

The critical normal load values for the onset of groove formation obtained from 1, 10, and 100 mm/s testing speeds are given in Figure 7. It is evident that the critical load for the onset of groove formation strongly depends on the rubber content, with a lower onset critical load for higher PBA rubber addition. This is mainly due to the fact that a higher rubber addition causes a lower compressive yield stress of ASA, which makes it easier for the scratch groove to form.

Onset of periodic cracking

The onset of periodic crack damage feature for ASA1 and ASA5 are shown in Figures 8 and 9, respectively. Figures 8(a) and 9(a) show the laser confocal optical images and Figures 8(b) and 9(b) represent the corresponding topographic height information of the samples. The material properties have a significant impact on scratch damage features. Jiang et al.[13] concluded that in ductile polymers, such as thermoplastic polyolefins (TPO), the scratch tip usually causes periodic plastic drawing and forms fish-scale pattern due to the stick and slip process. In contrast, brittle polymers, such as epoxy, generally show periodic cracking. Although the addition of 30 wt % PBA rubber in ASA5 is able to increase the ductility of the hosting SAN copolymer significantly (Fig. 2), there is still no discernable change observed in the periodic damage features between SAN[1] and ASA5.

Furthermore, it has been shown that the cracks formed perpendicular to the scratch direction are a consequence of the buildup of a tensile stress component parallel to the scratch direction in the region behind the scratch tip.[13] Unlike the compressive stress dominant scenario in the early stage of scratch, FEM analysis showed that the magnitude of the tensile stress quickly increase to a level sufficient to initiate cracking as the applied normal load increases. Figure 10 indicates the critical normal load values for the onset of periodic cracking formation of the neat SAN and various ASAs. The results reveal that increasing the rubber content reduces the resistance to periodic crack formation. This trend correlates well with the observation in tensile behavior where the tensile strength decreases with increasing the rubber content of the ASA systems (Fig. 2).

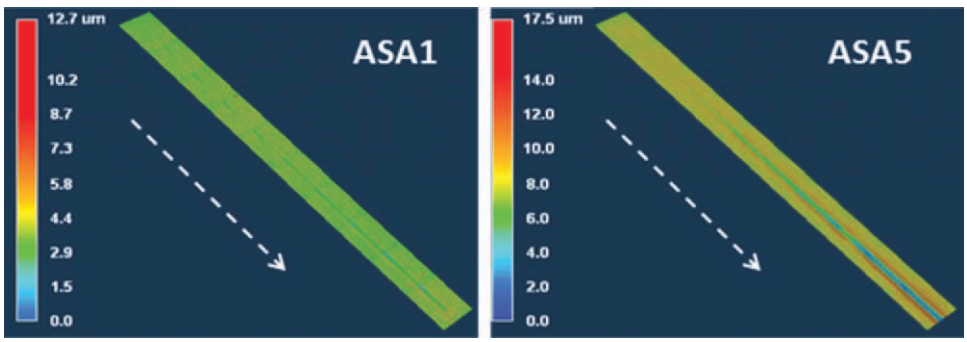

Figure 5 Height contour plots along the scratch paths of ASA1 and ASA5 via VLSCM. The scratch groove of ASA 5 deepens faster than in ASA1. [Color figure can be viewed in the online issue, which is available at wileyonlinelibrary.com.]

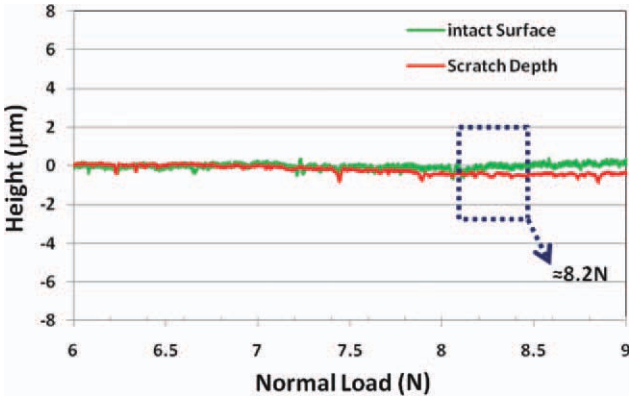

Figure 6 The groove height profiles in ASA1 before and after scratching. The first sign of height deviation from the scratch profile is denoted as the onset of groove formation. [Color figure can be viewed in the online issue, which is available at wileyonlinelibrary.com.]

Onset of plowing

Figure 11 illustrates the typical plowing deformation observed in ASA1 from top view and the corresponding height contour plot. At the final stages of the progressive load scratch test, the tensile stress components developed in front of the scratch tip possess the highest magnitude among other stress components.[13] This high tensile stress component whose direction is perpendicular to the moving scratch tip facilitates the cutting of the pile-up material in front of the scratch tip and reduces the stick-slip motion. As a result, a deep surface penetration of the scratch tip along with massive material removal develops. Figure 12 represents the critical normal load at the onset of plowing for the ASA systems. Increasing PBA rubber content reduces the critical normal load of plowing. However, it should

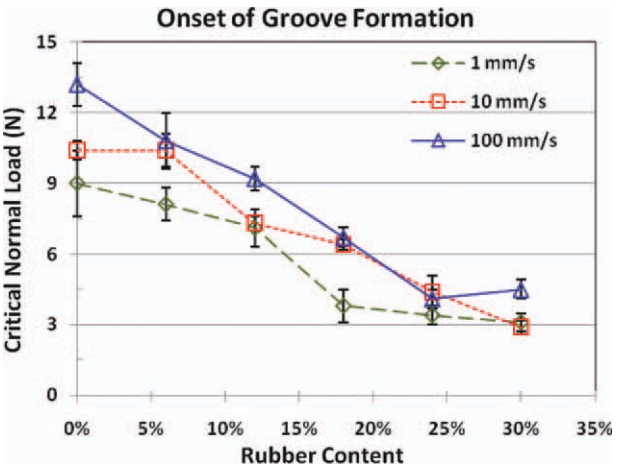

Figure 7 The critical normal loads at the onset of groove formation for the neat SAN and ASAs. Note the connecting lines between dots were added to emphasize their trends. [Color figure can be viewed in the online issue, which is available at wileyonlinelibrary.com.]

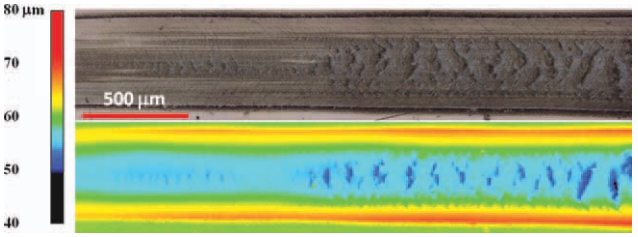

Figure 8 (a) Top view of the onset of periodic cracking for ASA1 tested at 1 mm/s. (b) The corresponding height contour plot. Note that the contrast of the images has been enhanced. [Color figure can be viewed in the online issue, which is available at wileyonlinelibrary.com.]

be noted that this trend is only seen at a scratch speed of 1 mm/s. Under higher scratch speeds of 10 mm/s and 100mm/s, the critical normal load for plowing formation appears to be independent of rubber content. The exact cause(s) for the discrepancy in the observed rate effect on the relationship between rubber content and the onset of plowing for the ASA systems is subjected to future investigations.

Scratch visibility analysis

From an aesthetic point of view, scratch visibility resistance of polymers is one of the most important factors in material selection for non-structural applications. Unfortunately, different individuals perceive color, contrast, and size of an object differently. It is imperative that machine-assisted determination of scratch visibility be implemented for reliable, objective, and repeatable analysis. Several types of image capture and analysis tools have been developed to provide quantitative scratch visibility evaluation.[26–28] A noted progress was recently made through the utilization of a desktop scanner and a commercially available software, termed automatic scratch visibility (ASV©) determination software,[28] for quantitative evaluation of scratch visibility resistance of polymers. Briefly, the ASV© acquires the scratched image from a sample via a desktop scanner and converts the RGB color components of the image into

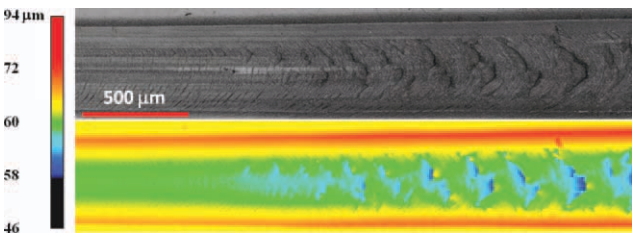

Figure 9 (a) Top view of the onset of periodic cracking for ASA5 tested at 1 mm/s. (b) The corresponding height contour plot. Note that the contrast of the images has been enhanced. [Color figure can be viewed in the online issue, which is available at wileyonlinelibrary.com.]

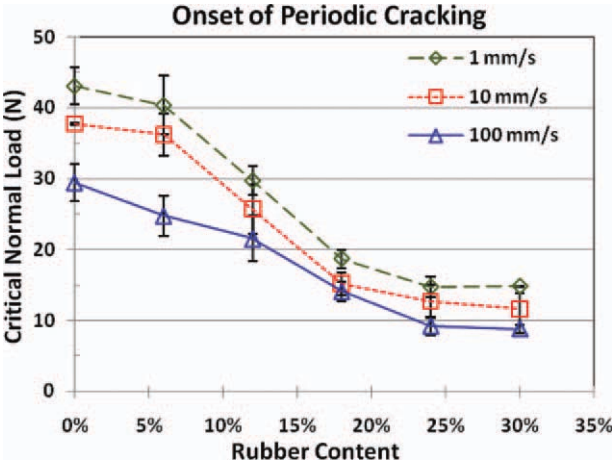

Figure 10 The critical normal loads showing the onset of periodic cracking for the neat SAN and all the ASA investigated. [Color figure can be viewed in the online issue, which is available at wileyonlinelibrary.com.]

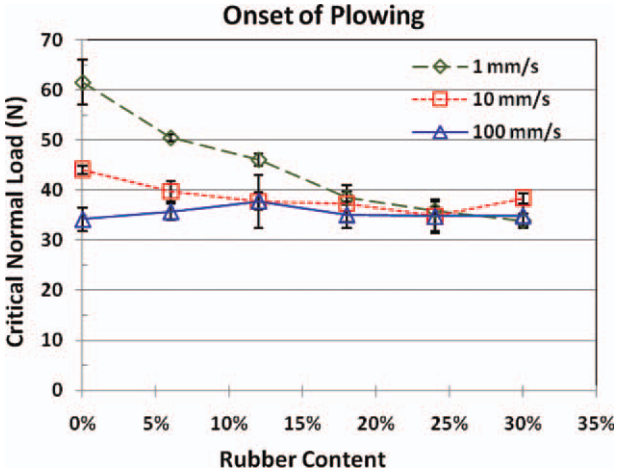

Figure 12 The critical normal loads showing the onset of plowing for the neat SAN and all the ASA investigated. [Color figure can be viewed in the online issue, which is available at wileyonlinelibrary.com.]

the respective brightness values to normalize the color-sensitivity variation among human observers. Moreover, it follows physiological principles that require the size of an object to be larger than 90 μm and a contrast level to be 2–3% different than the background[29,30] for the scratch to become visible.

The ASV© software along with a desktop scanner were utilized here to assess and compare the scratch visibility resistance of the ASAs. The "as-scanned" images of the scratches are shown in Figure 13. In the "as-scanned" images, a considerable difference in the onset of scratch visibility resistance among the ASA systems can be seen by the naked eye. In the ASV© processed images, the highlighted region denotes the visible scratch region. The white vertical lines indicate the onset of scratch visibility as determined by ASV©. Notably, the ASV© analysis reasonably reflects the naked eye observations, and more importantly, assesses the scratch visibility in a quantitative and reproducible fashion. It should be noticed that the criterion for surfaces with varying gloss needs to be different since scratches can be much more easily detected on high gloss surfaces than on low gloss surfaces. In this study, the contrast criterion was set at 2% for neat SAN and ASA1–ASA3, while 3% contrast criterion was used for ASA4 and ASA5 due to their less glossy surface nature (Table I).

The critical normal loads at the onset of scratch visibility for the ASA systems are plotted in Figure 14. It is evident that the scratch visibility resistance is reduced while increasing rubber content. This is expected since higher rubber content leads to lower yield stress in ASAs, which, in turn, causes a larger shoulder height alongside the scratch groove leading to earlier occurrence of scratch visibility.

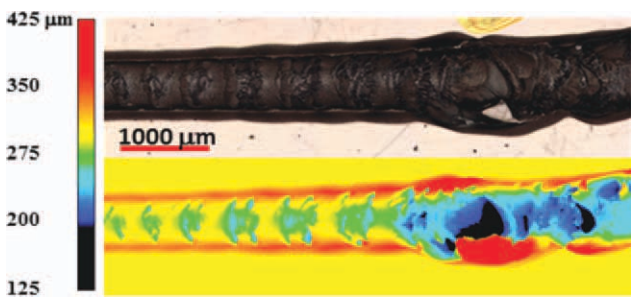

Figure 11 (a) Top view of the onset of plowing of ASA1 tested at 1 mm/s. (b) The corresponding height contour plot. Note that the contrast of the images has been enhanced. [Color figure can be viewed in the online issue, which is available at wileyonlinelibrary.com.]

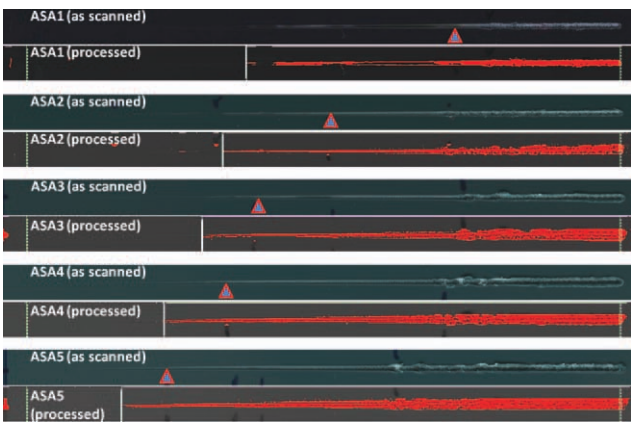

Figure 13 The scanned and via ASV processed images of ASAs tested at 1 mm/s. The onset of scratch visibility as determined by ASV is indicated by the vertical white lines. The triangular symbols in the scanned images denote the location for the onset of periodic cracking formation. [Color figure can be viewed in the online issue, which is available at wileyonlinelibrary.com.]

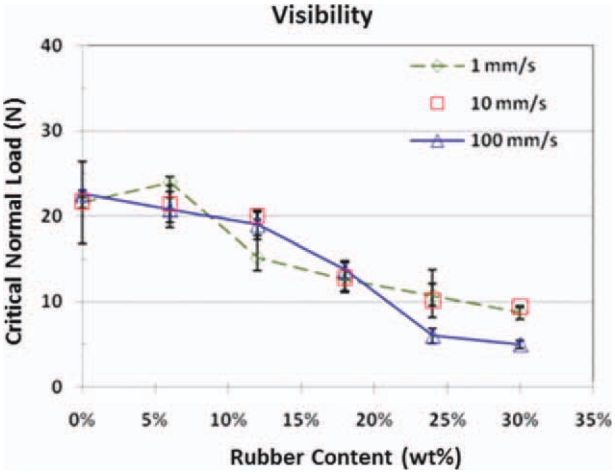

Figure 14 The critical normal loads showing the onset of scratch visibility for neat SAN and ASAs. [Color figure can be viewed in the online issue, which is available at wileyonlinelibrary.com.]

Effect of scratch speed on ASA scratch performance

Since polymers are viscoelastic in nature, scratch speed can significantly influence the critical normal load for the onset of various scratch deformations. This phenomenon has been observed in both brittle and ductile polymers, such as the brittle SAN systems[1,25] and the ductile TPOs.[11] Polymers usually exhibit a higher modulus, higher yield stress, and lower ductility when subjected to a higher rate of testing.[19,31] As expected, a higher scratch speed leads to a higher critical load for groove formation (Fig. 7). However, despite the strong relationship between the onset of periodic microcracking and tensile strength shown earlier, a higher scratch speed leads to a lower critical load for periodic crack formation (Fig. 10). Perhaps this is due to the decrease in ductility caused by higher scratch testing speed,[19] which facilitates the formation of microcracks. The exact reason behind this phenomenon is still unclear and is subjected to our further investigations.

It is also noted that, as shown in Figures 10 and 12, the effect of scratch speed on the critical load for periodic cracking and plowing formation becomes less significant in the ASAs containing more than 18 wt % rubber particles. This phenomenon is likely related to the fact that rate sensitivity on mechanical properties of polymers can be reduced by higher rubber content in polymers.[31] The lack of rate dependency on scratch visibility may be due to the physical origins responsible for scratch visibility, which cannot be explained by viscoelastic behavior of the polymers alone.

Scratch coefficient of friction

Scratch coefficient of friction (SCOF) discussed here is defined as the measured tangential force divided by the applied normal load. Figure 15 shows the plot of SCOFs of the ASA systems as a function of scratch distance. The results from SAN, ASA2, and ASA4 are not included to avoid redundancy. From Figure 15, noticeable differences in SCOF for ASA1 through ASA5 can be observed with ASA1 having the lowest SCOF up to the plowing transition region. This finding is consistent with our earlier observation where similar types of samples that exhibit better scratch resistance tend to possess lower SCOF.[1,9,10,12] In the plowing region, the magnitude of SCOF decreases with scratching speed. This may be due to the fact that the material is removed in a steady-state fashion, which lowers the SCOF.

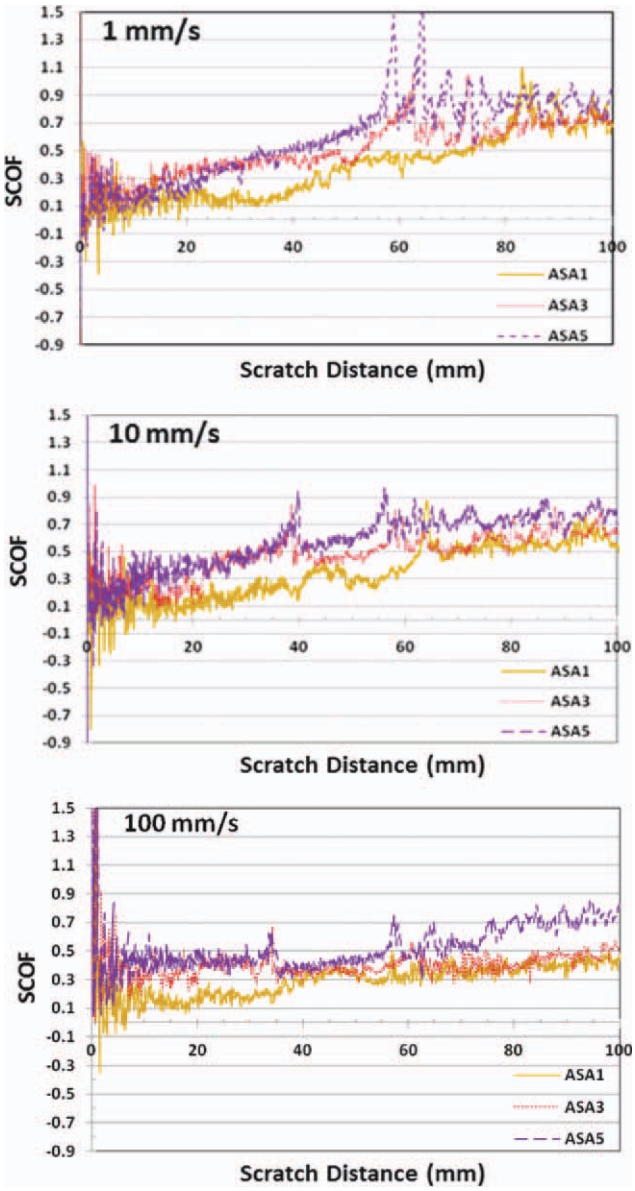

Figure 15 The SCOF of selected ASAs plotted against the scratching distance/(load). [Color figure can be viewed in the online issue, which is available at wileyonlinelibrary.com.]

Implication of the present study

The present study indicates that the addition of PBA rubber particles reduces the modulus and yield stress of the matrix, which lowers the critical load for groove formation, periodic crack formation, and scratch visibility. One possible remedy to the drawbacks of rubber toughening is to introduce nanosized rubber particles for toughening brittle polymer matrices. It has been shown that when nanosized rubber particles are introduced, significant improvements on fracture toughness and ductility can be achieved without reduction in modulus and yield stress.[32,33] It is also possible to introduce hybrid toughening approach to improve toughness, ductility, yield stress, and modulus of the matrix simultaneously.[34,35] Furthermore, since the fracture toughness and ductility is measured based on the bulk sample and the scratch performance is only affected by the surface layer of the sample, it is possible to retain scratch performance by altering the rheology of the rubber particles such that their impact to the surface properties of the polymer can be minimized. Efforts are currently underway to confirm whether the above approaches can indeed improve both scratch resistance and fracture toughness of polymers.

CONCLUSION

The rubber content effect on the scratch performance in ASAs has been studied. Incorporation of rubber particles generally decreases the scratch resistance of SAN and further deteriorates its scratch performance as the rubber concentration increases. The decrease in scratch resistance is strongly related to the reduction of tensile and compressive yield stresses and modulus in ASA systems, but not the enhanced ductility nor their impact strength. The current finding is consistent with our earlier FEM modeling and experimental observations. The scratch visibility was also evaluated by an ASV© software package to address the aesthetics retention of ASA samples. As expected, scratch visibility resistance of ASA polymers is inversely correlated with rubber content. Significant research is still needed to adequately utilize rubber particles addition for improving scratch resistance of polymers.

The assistance by Dr. Robert Browning and Mr. Peng Liu in scratch visibility evaluation is highly appreciated.

References

1. Browning, R.; Sue, H. J.; Minkwitz, R.; Charoensirisomboon, P. Polym Eng Sci 2011, 51, 2282.
2. Tabor, D. Br J Appl Phys 1956, 7, 159.
3. Guevin, P. R. J Coat Technol 1995, 67, 61.
4. Kody, R. S.; Martin, D. C. Polym Eng Sci 1996, 36, 298.
5. Chu, J.; Rumao, L.; Coleman, B. Polym Eng Sci 1998, 38, 1906.
6. Krupicka, A.; Johnansson, M.; Hult, A. Prog Org Coat 2003, 46, 32.
7. Wong, M.; Lim, G. T.; Moyse, A.; Reddy, J. N.; Sue, H. J. Wear 2004, 256, 1214.
8. Browning, R. L.; Lim, G.-T.; Moyse, A.; Sue, H.-J.; Chen, H.; Earls, J. D. Surf Coat Technol 2006, 201, 2970.
9. Jiang, H.; Lim, G. T.; Whitcomb, J. D.; Sue, H.-J. J Polym Sci Polym Phys Ed 2007, 45, 1435.
10. Jiang, H.; Browning, R.; Fincher, J.; Gasbarro, A.; Jones, S.; Sue, H. J. Appl Surf Sci 2008, 254, 4494.
11. Browning, R. L.; Jiang, H.; Moyse, A.; Sue, H. J.; Iseki, Y.; Othtani, K.; Ijichi, Y. J Mater Sci 2008, 43, 1357.
12. Moghbelli, E.; Browning, R. L.; Boo, W. J.; Hahn, S. F.; Feick, L. J. E.; Sue, H. J. Tribol Int 2008, 41, 425.
13. Jiang, H.; Browning, R.; Sue, H. J. Polymer 2009, 50, 4056.
14. Moghbelli, E.; Sun, L.; Jiang, H.; Boo, W. J.; Sue, H. J. Polym Eng Sci 2009, 36, 483.
15. Briscoe, B. J. Tribol Int 1998, 31, 121.
16. Briscoe, B. J.; Pelillo, E.; Sinha, S. K. Polym Eng Sci 1996, 36, 2996.
17. Maeda, K.; Bismarck, A.; Briscoe, B. J. Wear 2005, 259, 651.
18. Kim, H.; Keskkula, H.; Paul, D. R. Polymer 1990, 31, 869.
19. Steebrink, A. C.; Litvinov, V. M.; Gaymans, R. J. Polymer 1998, 39, 4817.
20. McKee, G. E.; Kistenmacher, A.; Goperrissen, H.; Breulmann, M. In Modern Styrenic Polymers; Scheirs, J.; Priday, D., Ed.; Wiley, 2002.
21. Kunststoff Information (2008) 1915:1.
22. ASTM International. ASTM D638, Annual Book of ASTM Standards; 1998.
23. ASTM International. ASTM D695, Annual Book of ASTM Standards; 1996.
24. ASTM International. ASTM D7027-05, Annual Book of ASTM Standards; 2005.
25. Zhang, L.; Li, J. C. M. Mater Sci Eng 2003, A344, 182.
26. Weon, J. I.; Song, S. Y.; Choi, K. Y.; Lee, S. G.; Lee, J. H. J Mater Sci 2010, 45, 2649.
27. Koch, T.; Machl, D. Polym Test 2007, 26, 927.
28. Jiang, H.; Browning, R. L.; Hossain, M. M.; Sue, H. J. Appl Surf Sci 2010, 256, 6324.
29. Buchsbaum, W. H. Color TV Servicing, 3rd ed.; Prentice Hall, 1975.
30. Roberts, M. Biology: A Functional Approach, 4th ed.; Nelson Thornes, 1986.
31. Yee, A. F.; Pearson, R. A. J Mater Sci 1986, 21, 2462.
32. Liu, J.; Sue, H. J.; Thompson, Z. J.; Bates, F. S.; Dettloff, M.; Jacob, G.; Verghese, N.; Pham, H. Macromolecules 2008, 41, 7616.
33. Liu, J.; Sue, H.-J.; Thompson, Z. J.; Bates, F. S.; Hillmeyer, M. A.; Dettloff, M.; Jacob, G.; Verghese, N.; Pham, H. Macromolecules 2010;43, 7238.
34. Sue, H.-J.; Gam, K. T.; Bestaoui, N.; Clearfield, A.; Miyamoto, M.; Miyatake, N. Acta Mater 2004, 8, 2239.
35. Sun, D.; Chu, C.-C.; Sue, H.-J. Chem Mater 2010, 22, 3773.
36. Biron, M. Thermoplastics and Thermoplastic Composites, Technical Information for Plastic Users; Elsevier Ltd, 2007.
37. Jiang, H.; Whitcomb, J. D.; Sue, H. J. Mechanical modeling of scratch induced periodic damage, In Proceedings of the 11th Annual SPE TPO Conference, Detroit, MI, 2009.